Opt Quant Electron
DOI 10.1007/s11082-015-0145-y

The influence of Ce doping on the structural and optoelectronic properties of RF-sputtered ZnO films

Manuel García-Méndez[1] · Ricardo Rangel Segura[2] · Víctor Coello[3] · Eduardo Martínez Guerra[4] · Álvaro Bedoya-Calle[5]

Received: 29 January 2015 / Accepted: 2 March 2015

Abstract Using X-ray diffraction, UV-Visible spectroscopy, XPS and photoluminescence (PL) measurements, the structural, optical and electronic properties of ZnO and Ce-doped ZnO thin films were investigated; the films were deposited on glass substrates by RF reactive-magnetron sputtering and post-annealed at 300 °C in an oxygen atmosphere. Under similar deposition conditions, both films crystallized into hexagonal würzite lattice structures. The pure ZnO film exhibited a c-axis preferential orientation, whereas the Ce-doped exhibited an a-axis preferential orientation. The films display uniform textured surfaces with columnar-like microstructures. The UV-Vis spectra showed high transparencies of 90 % on average for both films. Band gaps of $E_g = 3.23$ eV and $E_g = 3.27$ eV for pure and Ce-doped film, respectively, were measured. The doped film spectrum was shifted to the blue as a result of the Burstein-Moss effect. The XPS spectra show that the VB edge of the doped film shifts toward lower binding energy, at ~ 1.3 eV below E_F, while the VB edge of the pure film is located at ~ 2.0 eV below E_F. Additionally, Ce^{3+} and Ce^{4+} ions coexist in the ZnO matrix in fractions of ~ 70 and ~ 30 %, respectively. The PL spectra show that both types of ions induce extra electron states that allow multiple emission peaks in the blue–green region.

✉ Manuel García-Méndez
mgarcia@fcfm.uanl.mx

[1] CICFIM de la FCFM-UANL, Manuel L. Barragán S/N, Cd. Universitaria, CP. 66450 San Nicolás de los Garza, N.L., Mexico

[2] División de Estudios de Posgrado, Facultad de Ingeniería Química, UMSNH, Francisco j. Mújica S/N, CP. 58030 Morelia, Mich., Mexico

[3] CICESE Unidad Monterrey, Alianza Sur 203, Parque PIIT, CP. 66600 Apodaca, N.L., Mexico

[4] Centro de Investigación en Materiales Avanzados, S.C. (CIMAV), Av. Alianza Norte #202, PIIT, Nueva Carretera Aeropuerto Km. 10, CP. 66600 Apodaca, N.L., Mexico

[5] FIME de la UANL, Av. Universidad S/N, Cd. Universitaria, CP. 66450 San Nicolás de los Garza, N.L., Mexico

Published online: 18 March 2015

Keywords Zinc oxide films · RF sputtering · Optical properties · Electronic properties

1 Introduction

Zinc oxide (ZnO) is a binary transparent conducting oxide (TCO) with properties of great interest due to their basic scientific research and potential technological applications (Dondapati et al. 2013; Ammaih et al. 2014; Sachet et al. 2013; Suchea et al. 2006; Logothetidis et al. 2008; Frölich and Wegener 2011). ZnO has a würzite crystalline structure (lattice spacing $a_0 = 3.24$ Å and $c_0 = 5.20$ Å). ZnO also possesses a wide ordinary optical band gap (E_g) of 3.3 eV, which makes it transparent in the UV-Vis-NIR region, and a large exciton binding energy (60 meV), which enhances the luminescence efficiency of light emission (Dondapati et al. 2013; Gayen et al. 2011; Al-Kuhaili et al. 2012). This material has garnered much commercial and scientific interest compared with other TCO films, such as indium tin oxide (Minami 2005). The numerous advantages of ZnO include the tuning of its physical properties, its low cost, its abundance in the earth, its non-toxicity, and its compatibility with large-scale processes and relative easy fabrication (Logothetidis et al. 2008; Yang et al. 2006). Several techniques have been used to grow ZnO films, such as pulsed laser deposition (Sachet et al. 2013), DC reactive-magnetron sputtering (Suchea et al. 2006; Logothetidis et al. 2008), atomic layer deposition (Frölich and Wegener 2011), ZnO films deposited by RF magnetron sputtering depend on the deposition parameters involved in the growth process, such as the RF power, sputtering gas pressure, gas flow rate, and temperature. By adjusting these processing parameters, ZnO films with properties that are compatible with optical devices may be obtained (Al-Kuhaili et al. 2012; Lin et al. 2004; Kim et al. 2010b; Kapustianyk et al. 2007). Additionally, doping with selective elements can induce changes in the structural, electrical, optical, and electronic properties of ZnO films (Morinaga et al. 1997; Kim et al. 2010a; Joshi et al. 2010).

Among elements available for doping, such as Al, Cu, and Ag, (Kulyk et al. 2009), Ce has drawn interest in recent years due to the potential of Ce-doped ZnO films in optoelectronic applications, such as vacuum fluorescent and electroluminescent displays (Yang et al. 2014, 2008). It is mentioned in the literature that the emission of Ce-doped films is in either the UV or the visible region (Sofiani et al. 2006; Luo et al. 2012). When excited by UV light, the Ce-doped ZnO films emit violet, blue, green, and yellow, depending on the doping and crystal quality (Morinaga et al. 1997; Kim et al. 2010a; Joshi et al. 2010).

Therefore, more precise knowledge of the fine-tuning of RF-grown ZnO film structural and optoelectronic properties are needed due to the critical dependence of properties on deposition conditions, doping, and post annealing and given the potential applications of this type of films. In this work, undoped (ZnO) and cerium-doped zinc oxide (ZnO:Ce) films were deposited by RF magnetron sputtering. After deposition, the films were annealed in an oxygen atmosphere to minimize structural defects such as oxygen vacancies and interstitial zinc as well as to improve crystallinity and preferred orientation. The ZnO films were characterized using X-ray diffraction, UV-Vis spectroscopy, PL spectroscopy, and XPS. The effects of Ce on the structural, optical and electronic properties of the ZnO film were investigated.

2 Experimental

2.1 Experimental set-up for the deposition of films

Undoped and Ce-doped ZnO thin films were deposited by RF reactive-magnetron sputtering from 99.99 % pure metallic Zn and 99.99 % alloy $Zn_{95}Ce_5$ targets. The films were deposited on glass substrates in an ultra-high purity argon-oxygen atmosphere. Before deposition, both the substrate and the target were cleaned in an ultrasonic bath rinsed in acetone. The deposition chamber (a bell jar) was pumped down to a base pressure of 4.0×10^{-5} Torr. The gases were introduced through individual electronic mass-flow meters (Alborg). The target-substrate distance was kept constant at 5 cm, and a moveable shutter was placed between target and substrate. Plasma was then generated at an argon working pressure of 20 mTorr by applying a RF power of 30 W. The target was sputter cleaned for 5 min with the shutter protecting the sample. Once sputter cleaning was completed, the oxygen was introduced into the deposition chamber. The working pressure was maintained at $\sim$22 mTorr, while the oxygen and argon flow, during deposition, were 20 and 1 sccm, respectively. The thickness and deposition rate were monitored via a quartz crystal oscillator, and a final coating thickness of 300 and 340 nm were achieved in 30 min.The ZnO films were subjected to thermal annealing at temperatures of 100, 200 and 300 °C under an Ar:O_2 (90:10 %) mixture gas atmosphere. The annealing time was fixed in each case to 1 h and the working pressure was 22 mTorr. Several experiments were performed under the same conditions to ensure the reproducibility of results.

2.2 Characterization techniques

The XRD patterns were recorded with a Rigaku Miniflex II diffractometer in Bragg-Brentano geometry using a Cu-Kα radiation in a 2θ range with a step size of 0.02°. Surface microstructure and Root mean-square roughness (Rrms) of films were obtained from Atomic Force Microscopy analysis. Optical transmittance measurements were performed at the wavelength range of 300 to 900 nm with a Thermo-Scientific Evolution 600 UV-Vis spectrophotometer. Photoluminescence (PL) spectra were measured by a spectrofluorometer (FluoroMax-4, Jobin Yvon-SPEX) in the spectral range of 350–700 nm. The repetition rate of the Xe flash lamp was 25 Hz, and the integration window varied between 0.1 and 0.5 s at 325 nm. All measurements were performed in air at room temperature. XPS measurements were done with a Thermo Scientific K Alpha system which is equipped with monochromatized Al Kα anode (1486.6 eV). Spectra were acquired after cleaning the samples for 5 min using an argon sputtering ion gun at 10 mA and 3 KeV, on a 1 mm $\times$ 1 mm area. An argon beam charge neutralizer (flood gun) was employed to compensate for the charge up effect. Survey and high resolution (HR) spectra were collected with a resolution of 1 and 0.1 eV, respectively, with pass energies of 200 and 50 eV. The X-ray beam spot size was 400 μm^2. The binding energies were referenced to neutral adventitious C1s peak at 285.0 eV. Measured HR spectra of the O1s, Zn2p and Ce3d windows were analyzed after a linear background subtraction and fitted with Voight-type peaks. Elemental concentration was calculated using sensitivity factors included in the equipment software.

3 Results and discussion

Figure 1 shows the XRD spectra of the prepared films after annealing at 300 °C. In general, the XRD patterns indicate the polycrystalline nature of the ZnO and ZnO:Ce films. The high intensity of the peaks demonstrates the high quality of the films. The peak assignment corresponds to a würzite structure, JCPDS file 36–1451 ($a_0 = 3.24$ Å, $c_0 = 5.20$ Å). Regarding the ZnO film, the most intense (002) reflection indicates that the ZnO grew parallel to the c-axis of the hexagonal structure. Because the film surface is parallel to the substrate, the texture is the (0001) plane. Regarding this diffraction peak, the prominent (002) orientation is due to the lower surface energy compared to other planes (Al-Kuhaili et al. 2012; Mahmood et al. 2010; Bouderbala et al. 2009). A similar film growth direction is also achieved if the substrate is kept in a suitable position with respect to the target (Bouderbala et al. 2009). In the case of the ZnO:Ce film, the most intense (100) reflection indicates that the film has a [0002] preferential orientation parallel to the substrate.

The (002) plane has the lowest surface energy because it represents the closely packed planes in the hexagonal structure of ZnO. Such preferred orientation occurs to minimize the surface energy. The (100) planes are less stable than (002) planes and also exhibit a growth inclination with respect to the substrate. Hence, the surface texturing (100) is due to non-equilibrium growth.

The Bragg equation, $2d_{hkl}Sin\theta = n$, and the distance between planes for a hexagonal lattice relation

$$d_{hkl} = \frac{1}{\sqrt{\frac{4}{3}\left(\frac{h^2+hk+k^2}{a^2}\right) + \frac{l^2}{c^2}}} \tag{1}$$

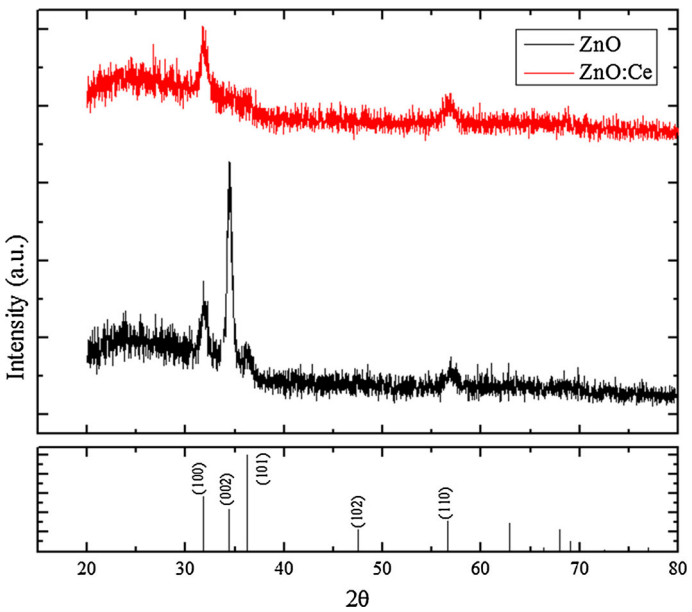

Fig. 1 X ray diffraction patterns of pure and Ce-doped ZnO films at 300 °C. The (002) plane is close-packed and has the lowest surface energy

was used to obtain the lattice parameters from the diffractograms. Afterwards, a multiple correlation analysis was performed by using a least-squares minimization. The initial values of a_0 and c_0 were taken from the JCPDS standard and introduced as fitting variables. Furthermore, the crystallite size, L, was estimated through the well-known Scherrer formula. For the ZnO film, the FWHM of the (002) peak was used for the calculations, whereas for the ZnO:Ce film, we used the FWHM, Γ, of the (100) peak. The results are presented in Table 1.

There, we can observe that the values of the lattice constants a_0 and c_0 for pure and doped ZnO are equivalent to those reported in the JCPDS standards (stress-free ZnO powder). Additionally, the 2θ positions of the (002) and (100) peaks for pure and doped ZnO, respectively, are not shifted to either higher or lower values. This fact indicates that the films have high crystalline qualities because no remarkable tensile or compressive stress was detected, even with the use of the dopant.

Our results regarding the changes in self-textures and crystalline quality of ZnO films due to the effects of doping and/or post annealing closely resemble others in the literature. For instance, Morinaga et al. (1997) report that Ce doping (1.5 % wt) improves the crystallinity and preferred orientation for RF-grown ZnO films and ensures that film growth remains in equilibrium. As Ce is an excellent oxidant, this metal promotes a tetrahedral coordination in the vapor phase and improves the (0001) texture. Sofiani et al. (2006) prepared Ce-doped ZnO films by spray pyrolysis, changing the Ce concentration from 0.8 to 12.3 % wt. They report that when the Ce content increases to approximately 2 % wt, the 2θ position of the (002) plane shifts toward to a lower angle. Conversely, for higher Ce concentrations, the 2θ peak shifts to a higher value. Thus, doping induces tensile stress. When the highly incorporated Ce^{3+} ions are not only substitutional but also interstitial, the crystalline qualities of the films degrade. Additionally, Zhu et al. (2011) found that post-annealing RF grown ZnO films in an H_2 atmosphere stabilizes the unstable (100) and (101) configurations, as an appropriate amount of H_2 as a sputtered gas can increase the grain size and can act as a mineralizer or a surfactant to improve the texturing of a growing ZnO film. Thus, different artifices can be used to stabilize apparently unstable surface configurations. In our case, the Ce content is not small enough to influence the (002) growth but it is large enough to stabilize the (100) growth on the ZnO:Ce film.

The sputtering conditions were near equilibrium to create a tetrahedral coordination. The Ce ions must be incorporated into the ZnO matrix by substituting Zn^{2+} ions, because no remarkable stress on film was detected. In addition, the annealing at 300 °C is also effective in removing both the metallized species and the sub-stoichiometric species in both films. For the ZnO film, the annealing stabilized the (002) growth, whereas for the ZnO:Ce film, the same mechanism stabilized the (100) growth. The average grain sizes were similar in both films; therefore, one can anticipate that the films will have a similar crystalline quality. Figures 2a, b shows AFM micrographs of ZnO and ZnO:Ce films, respectively. The films display uniform textured surfaces with columnar-like

Table 1 Summary of the structural parameters of the films

	2θ (hkl)	Γ (nm)	L (nm)	a (Å)	c (Å)
ZnO	34.4 (002)	0.48	17.8	3.25	5.2
ZnO:Ce	31.6 (100)	0.60	14.2	3.24	5.2

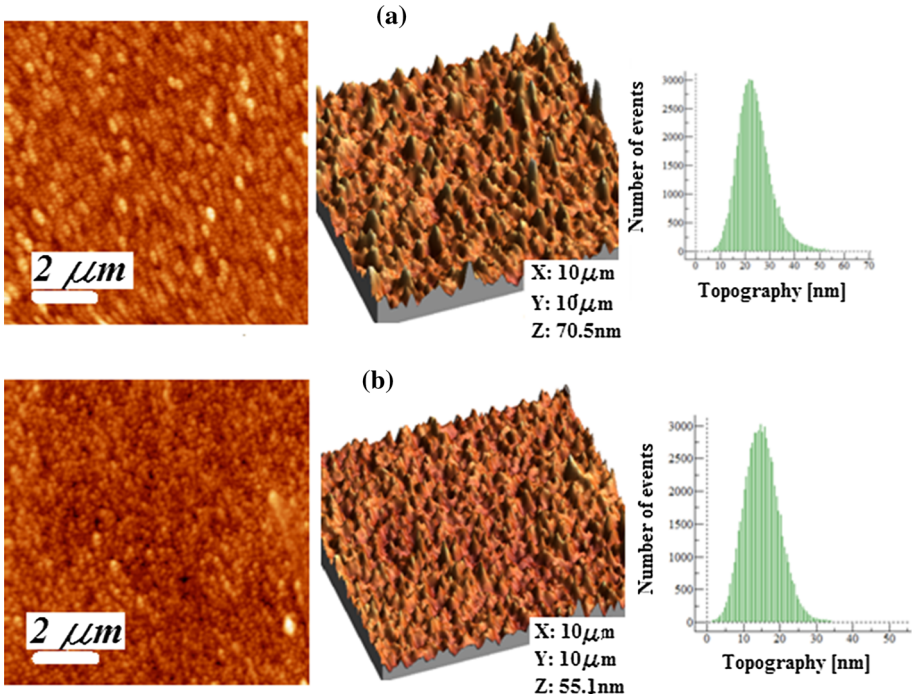

Fig. 2 AFM micrographs of **a** ZnO and **b** ZnO:Ce films

microstructures. The textured morphology is most likely due to the preferential growth orientation, which was confirmed by XRD measurements. The R_{rms} values of the pure and doped films were approximately 7.03 and 4.98 nm, respectively. The grain size and R_{rms} slightly decreased after Ce doping.

Figure 3 shows the transmittance spectra of films at 300 °C in the wavelength range of 300 to 900 nm. The optical band gap (E_g) were obtained by the Tauc method (inset).

At the onset of the absorption edge, the absorption coefficient α can be calculated from the relation:

$$\alpha = \frac{1}{d} Ln\left[\frac{100}{T(hv)}\right] \tag{2}$$

where T is the measured transmittance and d is the optical thickness (Youssef et al. 2009). The optical thickness and refractive index, n are extracted from T using the envelope method (Manifacier et al. 1976; Swanepoel 1983). By applying this method, optical thicknesses of $\sim$300 and $\sim$340 nm for ZnO and ZnO:Ce films, respectively, were obtained.

For a direct band gap semiconductor, E_g is obtained using the Tauc's relation:

$$(\alpha hv)^2 = A(hv - E_g) \tag{3}$$

where A is the edge width parameter. The optical band gap values are obtained by extrapolating the linear portion of the $(\alpha h)^2$ versus hv to $\alpha = 0$ (Ammaih et al. 2014; Suchea et al. 2006; Mahmood et al. 2010). Figure 3 shows that the average transmittance for both

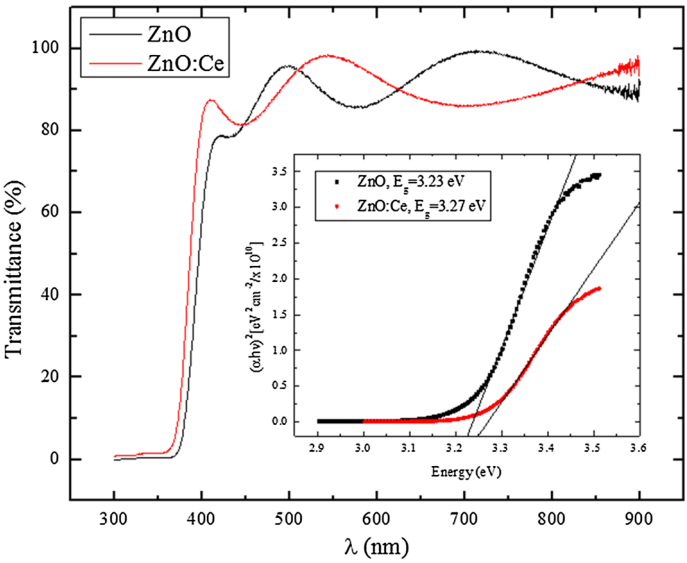

Fig. 3 Transmittance spectra of ZnO films at 300 °C. *Inset* $(\alpha hv)^2$ versus (hv) curves

samples was approximately 90 % in the visible wavelength region ($\sim$400–750 nm). In the absorption region, the absorption edge was observed to shift toward shorter wavelengths when introducing the Ce. The Ce-doped film shows a bump (shoulder) in the region of 300–360 nm. Such issues can be attributed to excitonic interactions of the extra electrons in the ZnO matrix provided by the Ce. This phenomenon has also been reported for ZnO films containing unreacted Zn^0 species and in ZnO films doped with Ce, Al and Co (Madhup et al. 2010; Yang et al. 2008). Band gaps of $E_g = 3.23$eV ($d = 300$ nm) and $E_g = 3.27$eV ($d = 340$ nm) were obtained from Tauc curves for pure and Ce-doped films, respectively. Band gap values of $\sim$3.23–3.26 eV have been previously reported for RF deposited ZnO films (Al-Kuhaili et al. 2012; Lin et al. 2004; Bouderbala et al. 2009; Zhu et al. 2011). Optical absorption studies show that the absorption edge of the doped films shifts towards blue region with a widening of the band gap at a higher energy. Such a feature is related to the rising Fermi level by filling more electrons in the conduction band (Burstein-Moss effect) (Dondapati et al. 2013; Kim et al. 2010b; Luo et al. 2012). When Ce atoms are incorporated into ZnO, both ions (Ce^{3+}, Ce^{4+}), whether in substitutional or interstitial sites, tend to increase the carrier concentration. Then, the lowest levels of the CB are partially filled, *i.e.*, the lowest state of the conduction band is blocked. Thus, the energy separation between the valence band (VB) maximum and the unfilled CB minimum is widened.

Figure 4 displays the XPS spectra of films. The HR′s of Zn2p and O1s for ZnO are included in Fig. 4a–b. The HRs of Zn2p, O1s and Ce3d for ZnO:Ce are included in Fig. 4c–e. Figure 4f shows the HR′s valence band of both samples.

In Fig 4a, c, we can observe that the zinc core level consists of two sublevels $(2p_{3/2}$ and $2p_{1/2})$ due to spin-orbit splitting. The $2p_{3/2}$ peak centered at 1021.38 eV (Fig. 4a) and 1020.48 eV (Fig. 4b) are attributed to the formation of Zn^{2+}, corresponding to the Zn-O bond in the ZnO lattice (Al-Kuhaili et al. 2012; Yang et al. 2008; Luo et al. 2012). The

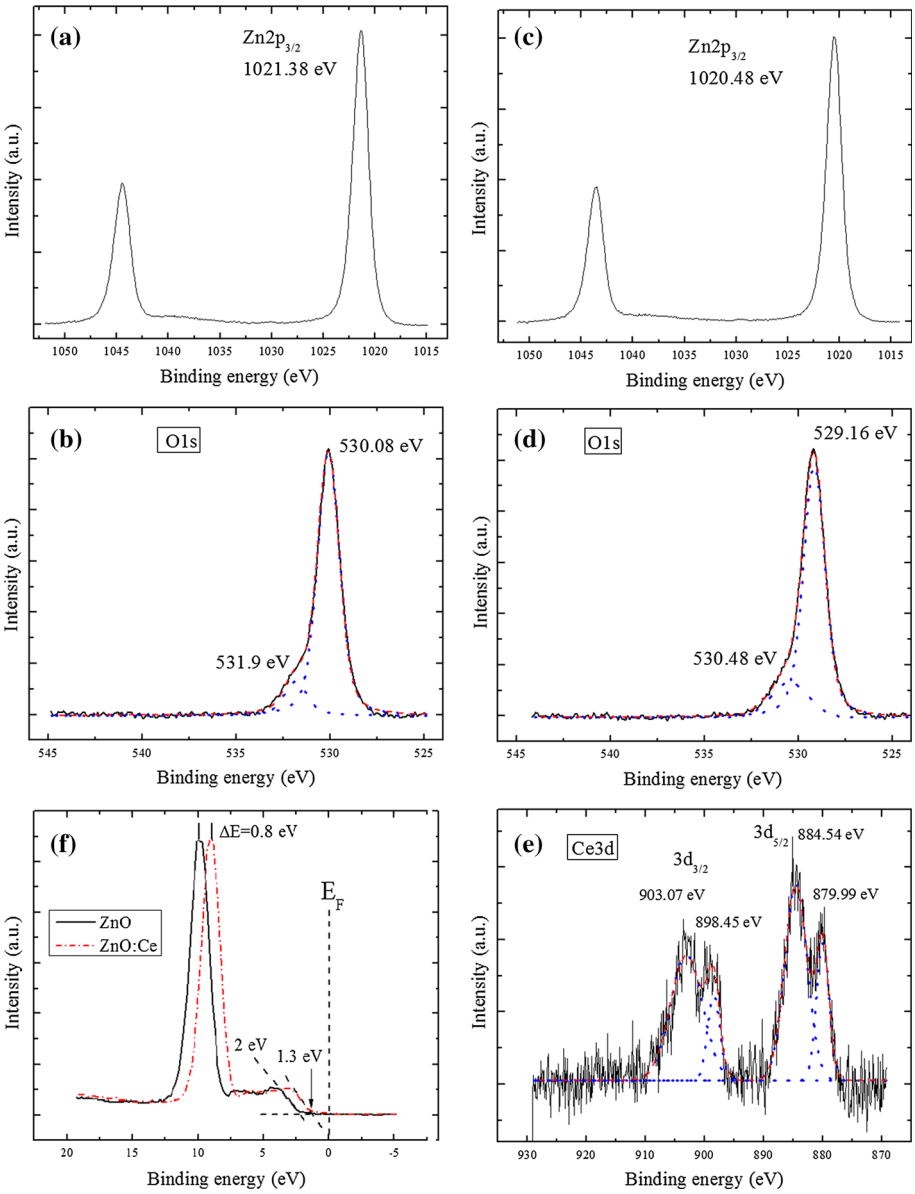

Fig. 4 XPS HR windows corresponding to **a** Zn2p, **b** O1s for un-doped ZnO; **c** Zn2p, **d** O1s, **e** Ce3d for Ce-doped ZnO; **f** valence band for pure and Ce-doped film

O1s peaks shown in Fig. 4b, d were each fitted with two components. The less intense components (531.9, 530.48 eV) are attributed to loosely bound oxygen on the surface, different from the lattice oxygen, as well as with photoemission from the lower oxygen valence state, e.g., O^{-}. The most intense components (530.08, 529.16 eV) are attributed to the Zn-O bond, as well with the photoemission of O^{2-} ions found in the bulk ZnO crystal

(Al-Kuhaili et al. 2012; Yang et al. 2008; Luo et al. 2012). The Ce3d spectrum was fitted using four components (Fig. 4e). The two peaks at 884.54 and 903.07 eV correspond to the $3d_{5/2}$ and $3d_{3/2}$ sublevels, respectively. They are attributed to Ce^{3+} ions in the ZnO lattice. The two peaks at 879.99 and 898.45 eV correspond to the $3d_{5/2}$ and $3d_{3/2}$ sublevels, respectively. They are attributed to Ce^{4+} ions in the ZnO lattice (Yang et al. 2008; Luo et al. 2012; Lang et al. 2010). Therefore, Ce^{3+} and Ce^{4+} ions coexist in the doped ZnO film. From the $Ce3d_{5/2}$ peak, a percentages of 71.8 and 28.1 % for Ce^{3+} and Ce^{4+} ions, respectively, were calculated. As Ce^{3+} and Ce^{4+} ions coexist in the doped ZnO film, both types of ions provide extra electrons to the lattice as carriers. As a result, the band gap structure will be modulated, giving rise to the blue shift of the absorption edge (Burstein-Moss effect).

From elemental concentration calculations, the stoichiometric proportion of the ZnO sample was found to be $Zn_{0.5}O_{0.49}$, whereas that corresponding to doped-ZnO was $Zn_{0.45}O_{0.46}$:$Ce_{0.078}$. Therefore, although no remarkable presence of structural defects was detected by X-ray characterization, the XPS measurements indicated that the growth of both films were non-stoichiometric, which slightly deviates from an ideal ZnO.

Figure 4f shows the valence band spectra of pure and doped films. The most intense transitions are attributed to the Zn3d band (Joshi et al. 2010; Calzolari and Nardelli 2013). The 3d peak positions are located at 9.88 and 8.99 eV for pure and doped film, respectively. The features detected at $\sim$5 eV below E_F (the VB edge) are attributed to the hybridization of the O2p and Zn4s orbitals (Joshi et al. 2010). Fitting a diagonal line and intercepting it with the horizontal axis, as sketched in the figure, can determine the shift of the VB edge. The VB edge of the doped film is observed to shift toward a lower binding energy, at $\sim$1.3 eV below E_F, while the VB edge of the pure film is located at $\sim$2.0 eV below E_F.

The PL spectra of the films are displayed in Figs. 5 and 6. On the graphs, the electromagnetic spectrum is included at the top to aid viewing of the emission signals.

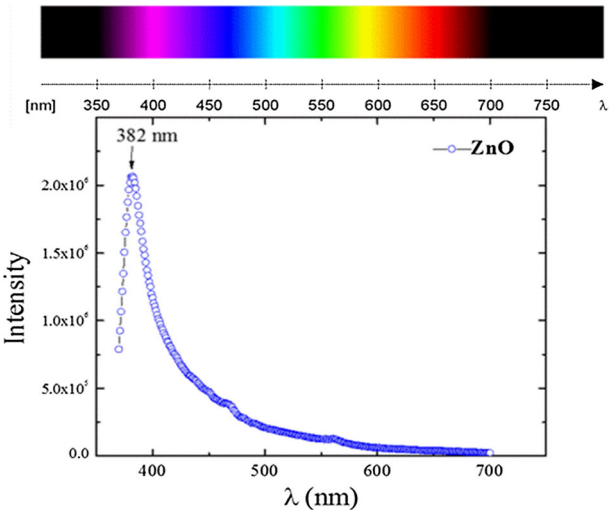

Fig. 5 Room temperature PL spectrum of undoped ZnO film

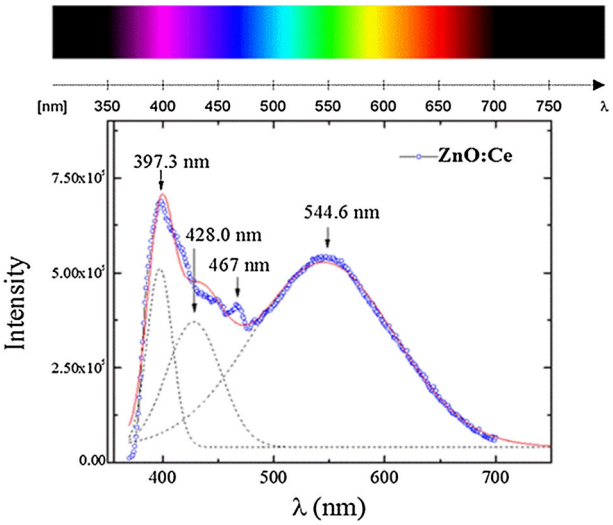

Fig. 6 Room temperature PL spectrum of Ce-doped ZnO film

Figure 5 shows the PL spectrum of the undoped ZnO film, where an intense UV peak is observed at 382 nm. The UV emission is an intrinsic property of the wurtzite ZnO and is attributed to the recombination of the photoexcited holes and the electrons (i.e., exciton generation) via a radiative process (Luo et al. 2012; Han et al. 2005; Kulyk et al. 2010). This mechanism is known as the near band edge (NBE) emission. Other less intense PL peaks at 467 nm (BE) and 561 nm (GE) are also observed. The dominance of a high intense PL peak at UV is related to the crystalline quality of the ZnO films, while the other peaks originate from the existence of defects and/or impurities related to local levels in the ZnO gap. Those effects steam from oxygen or interstitial zinc vacancies and are attributed to the non-stoichiometry of the ZnO film (Luo et al. 2012; Wang and Reynolds 2012; Li et al. 2000).

Figure 6 shows the PL spectrum of the Ce-doped ZnO film. The spectrum contains a characteristic UV emission at 397. 3 nm. The UV signal is slightly redshifted by $\sim$15.3 nm. Furthermore, this peak appears less intense and broadened, which is related to a more disordered structure due to the Ce inclusion. Broad emission at 544.6 nm (GE), with two signals at 428 nm and a small one at 467 nm, are also observed in the spectrum.

When Ce ions $(^{3+,4+})$ are incorporated into ZnO film, the bandgap structure of the ZnO film is substantially modulated and new emission centers are formed. Ce ions have been reported to introduce electron states into the band gap. These electron states are located closer to the lower edge of the conduction band (a new LUMO of lower energy), which results in a band gap reduction (Luo et al. 2012; Lang et al. 2010). Thus, when an electron is excited into the CB, it drops back to the VB. This process emits a photon shifted to the red.

In the literature, green emission is suggested to originate from electron-hole recombination at the defect sites due to electron transitions from the shallow donor level of the intrinsic defect centers, such as interstitial zinc to the valence or conduction band (Lang et al. 2010; Zhu et al. 2011; Bagnall et al. 1998). Additionally, the peaks at 428 nm and 467 nm are very similar in value to those reported by Luo et al. (2012) for DC sputtered

Ce-doped ZnO films. Both transitions can be ascribed to the electric-dipole allowed transition of the Ce^{3+} ions. These peaks are reported to originate from the lower 5d (^2D) excited state to the split $^2F_{5/2}$ and $^2F_{7/2}$ energy levels. In our sample, as Ce^{3+} and Ce^{4+} ions coexist in the ZnO matrix, the band gap was modified in such a way that multi-emission peaks are allowed in the blue-green region.

4 Conclusions

In summary, the structural, optical and electronic properties of RF sputter-deposited ZnO and Ce-doped ZnO films were examined after post annealing. Both films crystalized in würzite structure with lattice parameters very similar in value to the stress-free standard. The undoped film grew preferentially oriented at the [0002] direction, while the doped one grew preferentially oriented at the $[10\bar{1}0]$ direction. Both films possessed a similar crystalline quality, with a homogeneously textured surface. Transmittance of both films was high, approximately 90 % at the visible wavelength region ($\sim$400–750 nm), with a band gap of $E_g = 3.23$ eV and $E_g = 3.27$ eV for pure and Ce-doped films respectively. The absorption edge of the doped film was blue-shifted due to the Burstein-Moss effect. The XPS spectra showed the coexistence of Ce^{3+} and Ce^{4+} ions in a proportions of approximately 70:30 % in the host ZnO lattice. Both types of ions induce extra electron states that allows multi emission peaks in the blue–green region and a red-shift of the UV emission.

Acknowledgments This work was financed by CONACyT México, Grant 168234, and PAICyT-UANL, Grant CE671-11.

References

Al-Kuhaili, M., Durrani, S., Bakhtiari, I., Saleem, M.: Optical constants of vacuum annealed radio frecuency (rf) magnetron sputtering. Opt. Commun. **285**, 4405–4412 (2012)

Ammaih, Y., Lfakir, A., Hartiti, B., Ridah, A., Thevenin, M., Siadat, Pand: Structural, optical and electrical properties of ZnO:Al thin films for optoelectronic applications. Opt. Quantum Electron. **46**, 229–234 (2014)

Bagnall, D.M., Chen, Y.F., Shen, M.Y., Zhu, Z., Goto, T., Yao, T.: Room temperature excitonic stimulated emission from zinc oxide epilayers grown by plasma-assisted mbe. J. Cryst. Growth **605**, 184–185 (1998)

Bouderbala, M., Hamzaoui, S., Adnane, M., Sahraoui, T., Zerdali, M.: Annealing effect on properties of transparent and conducting ZnO thin films. Thin Solid Films **517**, 1572–1576 (2009)

Calzolari, A., Nardelli, M.: Dielectric properties and raman spectra of ZnO from a first principles finite-differences/finite-fields approach. Nat. Sci. Rep. **3–2999**, 1–5 (2013)

Dondapati, H., Santiago, K., Pradhan, A.K.: Influence of growth temperature on electrical, optical and plasmonic properties of aluminium: zinc oxide films grown by radio frequency. J. App. Phys. **114**, 143506 (2013)

Frölich, A., Wegener, M.: Spectroscopic characterization of highly doped ZnO films grown by atomic layer deposition for three dimensional infrared materials. Opt. Mater. Express **1–5**, 883–889 (2011)

Gayen, R., Sarkar, K., Hussain, S., Bhar, R., Pal, A.: ZnO films prepared by modified sol-gel technique. Indian J. Pure Appl. Phys. **49**, 470–477 (2011)

Han, W., Kang, S., Kim, T., Kim, D., Cho, W.: Effect of thermal annealing on the optical and electronic properties of ZnO thin films grown on p-si substrates. Appl. Surf. Sci. **245**, 384–390 (2005)

Joshi, A., Sahai, S., Gandhi, N., Radha Krishna, Y., Haranath, D.: Valence band and core-level analysis of highly luminescent ZnO nanocrystals for designing ultrafast optical sensors. Appl. Phys. Lett. **96**, 123102 (2010)

Kapustianyk, V., Turko, B., Kostruba, A., Sofiani, Z., Derkowska, B., Dabos-Seignon, S., Barwin ski, B., Eliyashevskyi, Y., Sahraoui, B.: Influence of size effect and sputtering conditions on the crystallinity and optical properties of ZnO thin films. Opt. Commun. **269**, 346–350 (2007)

Kim, J., Kim, M., Yu, J., Park, K.: H2/ar and vacuum annealing effect of ZnO thin films deposited by rf magnetron sputtering system. Curr. Appl. Phys. **10**, S495–S498 (2010a)

Kim, Y., Lee, W., Jung, D., Kim, J., Nam, S., Kim, H.: Optical and electronic properties of post annealed ZnO:Al films. Appl. Phys. Lett. **96**, 171902–171904 (2010b)

Kulyk, B., Sahraoui, B., Figa, V., Turkoc, B., Rudykc, V., Kapustiany, V.: Influence of ag, cu dopants on the second and third harmonic response of ZnO films. J. Alloys. Compd. **481**, 819 (2009)

Kulyk, B., Kapustianyk, V., Tsybulskyy, V., Krupka, O., Sahraoui, B.: Optical properties of ZnO/pmma nanocomposite films. J. Alloys. Compd. **502**, 24–27 (2010)

Lang, J., Han, Q., Yang, J., Li, C., Li, X., Yang, L., Zhang, Y., Gao, M., Wang, D., Cao, J.: Fabrication and optical properties of Ce-doped ZnO nanorods. J. Appl. Phys. **107**, 074302–074306 (2010)

Li, W., Mao, D., Zhang, F., Wang, X., Liu, X., Zou, S., Zhu, Y., Li, Q., Xu, J.: Characteristics of ZnO:Zn phosphor thin films by post-deposition annealing. Instrum. Methods Phys. Res. B **169**, 59–63 (2000)

Lin, S., Huang, J., Lii, D.: The effects of r.f. power and substrate temperature on the properties of ZnO films. Surf. Coat. Technol. **176**, 173–181 (2004)

Logothetidis, S., Laskarakis, A., Kassavetis, S., Lousinian, S., Gravalidis, C., Kiriakidis, G.: Optical and structural properties of ZnO for transparent electronics. Thin Solid Films **516**, 1345–1349 (2008)

Luo, Q., Wang, L., Guo, H., Lin, K., Chen, Y., Yue, G., Peng, D.: Blue luminiescence from Ce-doped ZnO thin films prepared by magnetron sputtering. Appl. Phys. A **108**, 239–245 (2012)

Madhup, D., Subedi, D., Huczko, A.: Influence of doping on optical properties of ZnO nanofilms. Optoelectron. Adv. Mater. **4–10**, 1582–1586 (2010)

Mahmood, A., Ahmed, N., Raza, Q., Khan, T., Mehmood, M., Hassan, M., Mahmood, N.: Effect of thermal annealing on the structural and optical properties of ZnO thin films deposited by the reactive e-beam evaporation technique. Phys. Scr. **82**, 065801–065808 (2010)

Manifacier, J., Gasiot, J., Fillard, J.: A simple method for the determination of the optical constants n, k and the thickness of a weakly absorbing thin film. J. Phys. E Sci. Inst. **9**, 1002–1004 (1976)

Minami, T.: Transparent conducting oxide semiconductor for transparent electrodes. Semicond. Sci. Technol. **20**, S35–S44 (2005)

Morinaga, Y., Sakuragi, K., Fujimura, N., Ito, T.: Effect of Ce doping on the growth of ZnO thin films. J. Cryst. Growth **174**, 691–695 (1997)

Sachet, E., Losego, M., Guske, J., Franzen, S., Maria, J.: Mid-infrared surface plasmon resonance in zinc oxide semiconductor. Appl. Phys. Lett. **102**, 051111–051114 (2013)

Sofiani, Z., Derkowska, B., Dalasinski, P., Wojdyla, M., Dabos-Seigon, S., Lamrani, M., Dghoughi, L., Bala, W., Addou, M., Sahraoui, B.: Optical properties of ZnO and ZnO:Ce layers grown by spray pyrolysis. Opt. Commun. **267**, 433–439 (2006)

Suchea, M., Christoulakis, S., Moschovis, K., Katsarakis, N., Kiriakidis, G.: ZnO transparent thin films for gas sensor applications. Thin Solid Films **515**, 551–554 (2006)

Swanepoel, R.: Determination of the thickness and optical constants of amorphous silicon. J. Phys. E Sci. Inst. **16**, 1214–1222 (1983)

Wang, D., Reynolds, N.: Photoluminescence of zinc oxide nanowires: the effect of surface band bending. ISRN Condens. Matter Phys. **2012**, 1–6 (2012)

Yang, J., Gao, M., Yang, L., Zhang, Y., Lang, J., Wang, D.: Low-temperature growth and optical properties of Ce-doped ZnO nanorods. Appl. Surf. Sci. **255**, 2646–2650 (2008)

Yang, Y., Sun, X., Chen, B., Xu, C., Chen, T., Sun, C., Tay, B., Sun, Z.: Refractive indices of textured indium tin oxide and zinc oxide thin films. Thin Solid Films **510**, 95–101 (2006)

Yang, Y., Li, Y., Wang, C., Zhu, C., Lv, C., Ma, X., Yang, D.: Rare-earth doped ZnO films: a material platform to realize multicolor and near-infrared electroluminescence. Adv. Opt. Mater. **2–3**, 240–244 (2014)

Youssef, S., Combette, P., Podlecki, J., Al Asmar, R., Foucaran, A.: Structural and optical characterization of ZnO thin films deposited by reactive rf magnetron sputtering. Cryst. Growth Des. **9**, 1088–1094 (2009)

Zhu, B., Wang, J., Zhu, S., Wu, J., Wu, R., Zeng, D., Xie, C.: Influence of hydrogen introduction on structure and properties of ZnO thin films during sputtering and post annealing. Thin Solid Films **519**, 3809–3815 (2011)